Crystal structure prediction for supersaturated AZO : the case of $Zn_3Al_2O_6$

Kim Rijpstra,[a] Stefaan Cottenier,[a b‡], Michel Waroquier [a] and Veronique Van Speybroeck [a]

Received Xth XXXXXXXXXX 20XX, Accepted Xth XXXXXXXXX 20XX
First published on the web Xth XXXXXXXXXX 200X
DOI: */*****

Increasing the Al-concentration in Al-doped ZnO (AZO) is one way of improving the conductivity of this transparent conductive oxide (TCO). Beyond a certain concentration, an unwanted secondary phase develops with a low conductivity. Its stoichiometry is $Zn_3Al_2O_6$, and its crystal structure has not yet been convincingly determined. By applying unbiased *ab initio* structure prediction tools, we predict the crystal structure of $Zn_3Al_2O_6$ to be monoclinic with space group Pm. It can be described as a nanofabric, with onedimensional Al_2O_3-wires penetrating a ZnO-matrix. This crystal has a formation energy that is lower than any structure proposed before, and is consistent with all available experimental information. Knowledge of the nature of this phase can help to avoid its formation and therefor to engineer AZO crystals with an increased level of Al-doping and associated increased conductivity.

1 Introduction

Over the past decades, transparent conducting oxides [1–5] have made their way into a variety of applications [6]. Solar cells, energy-conserving windows and flat-panel displays are among the best known ones. Three major material families with TCO properties are SnO_2, ITO (indium-tin oxide, In_2O_3:Sn) and ZnO. The former two are dominant in terms of the yearly produced volume, but as they contain expensive (In) and/or noxious (Sn) elements, alternatives are welcome. Intrinsic or doped ZnO has been optimized to performance levels that make it a viable substitute for several applications [4,7]. The figure of merit for TCO's is the ratio of the electrical conductivity to the optical absorption coefficient [6]. Al-doped ZnO (a.k.a. AZO) has been produced with an electrical conductivity as high as 1.2×10^4 S/cm, making its figure of merit to rival with the one of ITO [6,8,9]. Attempts to increase conductivity in AZO even further were made by aiming at an optimal distribution of the Al dopants over the sample, which can, for example, be achieved by Atomic Layer Deposition (ALD) [10–14]. In the course of such studies, a wide range of Al-concentrations was scanned, up to 25 at.% Al (as common in this field, at.% refers to the Al to Zn ratio) [11,14–16]. This largely surpasses the solubility limit of Al in ZnO, which lies between 0.1 and 0.5 at.% [17–21]. It has been observed that beyond 3-6 at.% Al, the conductivity drops again [11,15,22]. Yoshioka et al. [23,24] proposed the following explanation for this observation: beyond the solubility limit, a fraction of the sample adopts a new metastable crystal structure, that has a lower conductivity. In analogy to what is known about the ZnO-In_2O_3 system, they postulated for this metastable phase the same crystal structure as the one observed for the series of homologous phases $(ZnO)_m(In_2O_3)$ ($m \geq 3$). This is a 'nano-laminated' structure, that is shown schematically in Fig. 1-(a) for $m = 3$. It is formed by alternations of 3 atomic layers with the nominal composition InO_2 (AlO_2) and 4 atomic layers that are taken from ZnO. In the latter layers, 25 at.% of the Zn-positions are randomly substituted by In (Al). Yoshioka *et al.* examined this structure by Density Functional Theory, and observed (1) that its formation energy is smaller than the formation energy for Zn-vacancy defects (which were suggested before to be responsible for the conductivity decrease), (2) that it shows an expansion in the c-direction with respect to ZnO doped with substitutional Al, which is consistent with experimental observations by X-ray diffraction, and (3) that the 4, 5 and 6-coordinated Al-sites which appear in this crystal structure lead to a computed XANES-spectrum that is more consistent with the experimentally observed spectra. This proposal by Yoshioka *et al.* has been rapidly accepted by the community [5,11,13,15,25,26]. In particular, the presence of the homologous phase with $m = 3$ was claimed to be observed experimentally by at least two groups using XANES [27,28].

In this paper, we will show that a different metastable crystal structure can account equally well for the various experimental observations, while its formation energy is smaller than the one for the homologous phase. It is therefore more likely to occur. As we came to this conclusion by applying systematic crystal structure prediction tools, it is not very likely that yet another metastable structure with even lower formation energy exists. Knowing exactly which metastable phase(s) are formed in the supersaturated regime offers an additional handle to engineer (delay) in a systematic way their formation.

This paper is illustrative of the role *ab initio* crystal structure prediction, a tool developed during the past decade in the theoretical condensed matter community[29–31], can play in crystal engineering problems.

Sec. 2 gives technical details about the computational tools that are used. In Sec. 3 we examine crystal structure candidates that are inspired by structures that are known in chemically similar systems. In Sec. 4, an evolutionary algorithm is applied to find the most favourable crystal structure in a systematic, unbiased way. The final structure is checked against the available experimental evidence in Sec. 5.

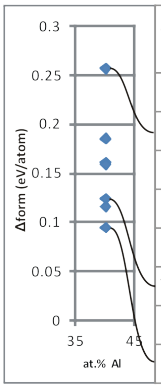

Source	Original Composition	Symmetry	Δform (eV/atom)
ICSD 409688	$Hg_3(BO_3)_2$	$R\bar{3}cH$	0.420
ICSD 240724	$Cd_3(BO_3)_2$	Pnnm	0.257
ICSD 14240	$Zn_3(BO_3)_2$	I12/c1	0.186
ICSD 155113	$Zn_3(BO_3)_2$	C12/c1	0.161
ICSD 155112	$Zn_3(BO_3)_2$	$P\bar{1}$	0.160
Yoshioka et al.	$In_2Zn_3O_6$	$R\bar{3}mH$	0.128
ICSD 655835	$In_2Zn_3S_6$	P3m1	0.117
USPEX, this work		Pm	0.095

Fig. 2 Formation energies of $Zn_3Al_2O_6$-polymorphs with respect to ZnO and gahnite. Left: graphical representation. In the table at the right, the first column gives either the ICSD number of the structure or the source where the structure was found, the chemical formula corresponding to the original crystal, the space group symbol and the value of the formation energy.

2 Computational details

All first principles calculations in this work have been performed within the density-functional theory (DFT) framework[32–34], using the Perdew-Burke-Ernzerhof exchange-correlation functional[35,36]. Actual calculations were made by the Projector Augmented Wave (PAW) method as implemented in the VASP code[37–39], using a 520 eV cut-off energy and Monkhorst-Pack grids **with a density of 600 points per Å^{-3}.** This guarantees a numerical accuracy that is better than 2 meV/atom on energy differences. During geometry optimizations, cell shape, volume and atomic positions were optimized, the latter until forces were smaller than 0.01 eV/Å. **A phonon calculation for the final structure was performed via the linear response method on a $2\times2\times2$ supercell, with tightly converged energies and forces.** Several cases were cross-checked by the augmented planewaves+local orbitals (APW+lo) method[34,40,41] as implemented in the WIEN2k package[42], leading to essentially identical results. **Within WIEN2k, muffin tin radii of R_{mt}^{Al}=R_{mt}^{O}=1.58 a.u. and R_{mt}^{Zn}=1.84 a.u. were used, together with a basis set size determined by $R_{mt}^{min}K_{max}$=7.0. Theoretical Al K-edge XANES spectra were calculated by WIEN2k as well, taking into account an Al 1s core-hole in supercells with 112 atoms for $ZnAl_2O_4$ and with 132 atoms for $Zn_3Al_2O_6$. The computed XANES spectra were broadened by a Lorentzian function with a characteristic width of 1 eV.** For crystal structure prediction by evolutionary search, the USPEX[29,43] code was used in combination with VASP.

3 Structure prediction by chemical similarity

Throughout this paper, we focus on one stoichiometry: $Zn_3Al_2O_6$. This is identical to the stoichiometry of the homologous phase $(ZnO)_m(Al_2O_3)$ with $(m = 3)$. The question we want to answer is: given this stoichiometry, what is the crystal structure that minimizes the total energy of the compound? One – limited – way of addressing this question is to scan a database of experimental crystal structures for all crystals with $A_3B_2C_6$ stoichiometry, where A is any element from group IIB of the periodic table (the group of Zn), B is any element from group IIIA (the group of Al) and C is any element from group VIA (the group of O). Only structures where each position is uniquely occupied by one element are considered. The Inorganic Crystal Structure Database[44] contains 6 different crystals of this kind, which are listed in Fig. 2. After replacing A by Zn, B by Al and C by O, a full geometry optimization of the cell is performed by VASP. The formation energy per formula unit of these crystals with respect to decomposition into the stable crystals ZnO and $ZnAl_2O_4$ (gahnite) is given by:

$$E_{\text{form}} = E[Zn_3Al_2O_6] - 2E[ZnO] - E[ZnAl_2O_4] \quad (1)$$

Positive formation energies mean that the decomposition into ZnO and $ZnAl_2O_4$ lowers the energy, such that the $Zn_3Al_2O_6$ crystal is only metastable. The formation energies are plotted in Fig. 2. Clearly, all crystals we found in this way are metastable. Fig. 2 shows the formation energy for the homologous phase model as well. Interestingly, one of these crystals – P3m1 – has an energy that is slightly lower than the one of the homologous phase model. It is actually similar to the homologous phase structure: AlO_2 layers separated by ZnO-layers, in which one Zn atom is replaced by Al in an ordered way.

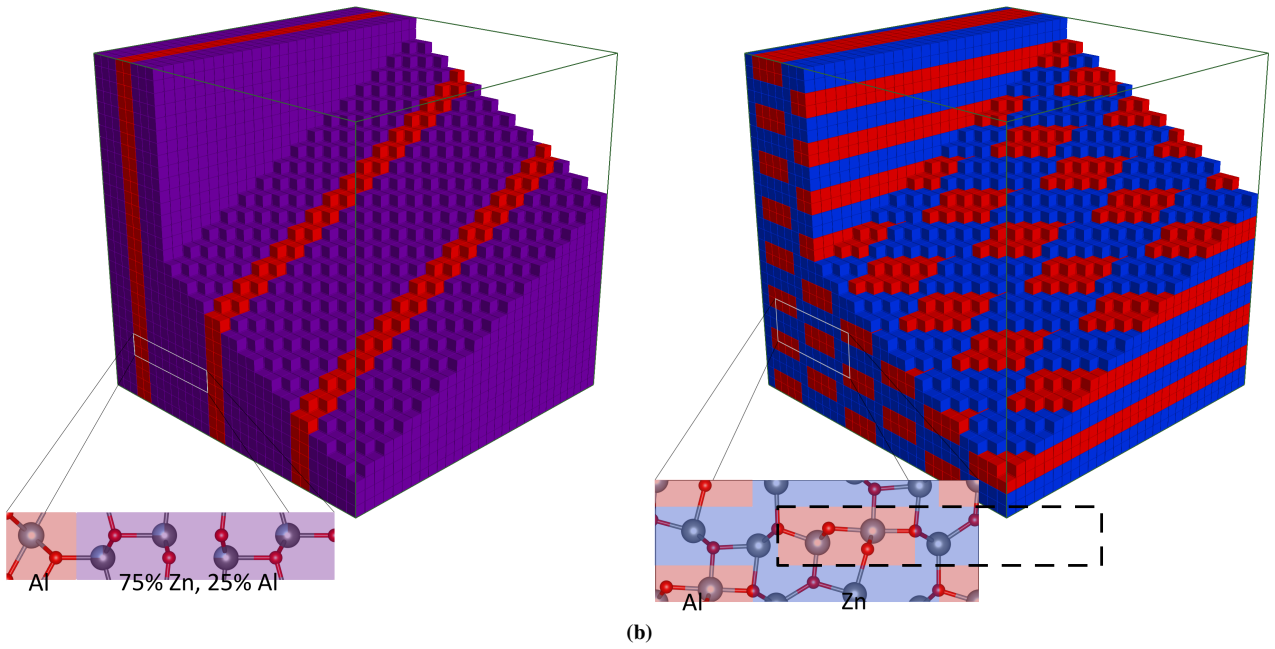

(a) **(b)**

Fig. 1 (a) Representation of the nanolaminated $Zn_3Al_2O_6$ structure proposed by Yoshioka *et al.* The rectangle contains one formula unit. The red (small) layers have as composition AlO_2. The purple (thick) layers are made of ZnO, with 25% of the Zn-positions randomly replaced by Al. What is not explicitly shown in this picture is an in-plane shift of the ZnO layer at the AlO_2 layers, such that only after the 3^{th} AlO_2 layer periodicity is reached. (b) Representation of the $Zn_3Al_2O_6$ nanofabric found by an evolutionary algorithm. The rectangular cell contains two primitive unit cells, the latter containing one formula unit. A basic building block is indicated by the dashed rectangle in the inset. This crystal can be described as a ZnO matrix (blue) that is penetrated by parallel and non-touching Al_2O_3 wires (red).

4 Structure prediction by an evolutionary algorithm

Searching the lowest-energy crystal structure for a given stoichiometry by looking at chemically similar systems is useful, yet incomplete. Perhaps the system under consideration can lower its energy by adopting a very different structure? It has been shown in the recent literature how evolutionary algorithms can be used in combination with DFT for a truly unbiased structure prediction[29–31] **: starting from a set of randomly generated crystals that mate and produce offspring, a selection procedure based on survival of the fittest produces after a few generations a crystal that is 'most adapted', i.e. that has the lowest possible total energy.** We applied the USPEX evolutionary algorithm[29,43] in combination with the VASP DFT code **as the the "quantum engine" that provides the total energies, in order** to find the lowest-energy crystal structure for the $Zn_3Al_2O_6$-stoichiometry. Runs were performed with one and two formula units per unit cell, always resulting in the structure that is shown in Fig. 1-(b). Its crystallographic information is given in Tab. 1. It has a formation energy that is 22 meV/atom lower than the one of the best structure found before. A Γ-phonon calculation showed all frequencies to be positive, which is a necessary condition for a crystal to be dynamically stable. To the best of our knowledge, no structure prototype of this kind was known before.

One can understand this structure as a way to enhance the mixing of Al_2O_3 and ZnO. Its basic building block is a rectangle that contains exactly one formula unit (indicated in Fig. 1-(b)). This column has a narrow Al-rich part with composition Al_2O_3 and a thicker Zn-rich part with composition ZnO. This building block is repeated in such a way – see Fig. 1-(b) – that isolated parallel Al_2O_3 wires penetrate a ZnO matrix. Instead of distinct AlO_2 layers separating regions of ZnO:Al (the nanolaminated homologous phase), this structure can be characterized as separate Al_2O_3-threads woven into a ZnO-medium – see Fig. 1-(b). This crystal is a nanofabric rather than a nanolaminated structure. In this way, the interface area between Al_2O_3 and ZnO is considerably increased.

5 Comparison with experiment

Two of the three arguments of Yoshioka *et al.* to prefer the homologous model structure over Zn-vacancy models, are straightforwardly satisfied as well by the structure proposed here: its formation energy is lower than the one of any other examined structure (including the homologous model), and it has interplanar distances of 2.72 Å, which is 2.6 % increased compared to the $d(002)$-spacing in wurtzite ZnO. The latter is in agreement with the experimentally observed interplanar distance increase upon Al-doping[23]. **The third argument was a comparison of experimental and theoretical**

Table 1 Crystallographic information for the structure that emerged as the best metastable $Zn_3Al_2O_6$crystal with at most two formula units per unit cell. A cif file is available from the Crystallographic Open Database[45,46] (COD) (entry 3000024)

space group		Pm (ITA=6)		
a		7.6519 Å		
b		5.4473 Å		
c		3.2419 Å		
γ		109.71°		
element	Wyckoff	x	y	z
Al	2c	0.00019	0.00153	0.00000
Al	2c	0.34071	0.07075	0.50000
O	2c	0.36540	0.75821	0.50000
O	2c	0.27101	0.15528	0.00000
O	2c	0.58613	0.30139	0.50000
O	2c	0.03179	0.86859	0.50000
O	2c	0.73719	0.86345	0.00000
O	2c	0.98569	0.33677	0.00000
Zn	2c	0.59532	0.68234	0.50000
Zn	2c	0.70661	0.22141	0.00000
Zn	2c	0.11022	0.53682	0.50000

XANES spectra. We reproduce in Fig. 3-(b) the experimental XANES spectrum (red) published by Yoshioka *et al.* for an AZO-sample with 19 at.% Al produced by pulsed laser deposition, as well as their theoretical XANES spectrum for the homologous phase structure (dotted grey). Yoshioka *et al.* concluded that this theoretical spectrum satisfactorily reproduces the overall shape of the experimental spectrum as well as the relative heights of the three major peaks (the latter indicated by arrows in the picture). The red line in Fig. 3-(b) is the newly computed theoretical XANES spectrum for the crystal structure that emerged from our evolutionary search (Tab. 1). It is remarkably similar to the computed XANES spectrum of the homologous phase, only shifted to lower energies by about 2 eV. Therefor, all arguments about the relative heights of the peaks hold equally well. Moreover, the onset of the experimental spectrum (position of the first peak) is much better described. Yoshioka *et al.* invoked an additional phase of Al-atoms near a Zn-vacancy to explain this feature. As a quality cross-check, Fig. 3-(a) shows the experimental XANES spectrum for the stable $ZnAl_2O_4$-phase (gahnite), compared with the theoretical spectra by Yoshioka *et al.* and by us. The two theoretical spectra nearly coincide, which implies that also the XANES spectrum for the new $Zn_3Al_2O_6$-structure has been computed in a technically correct way.

As the underlying reason why the homologous phase model yields to interplanar distances and XANES spec-

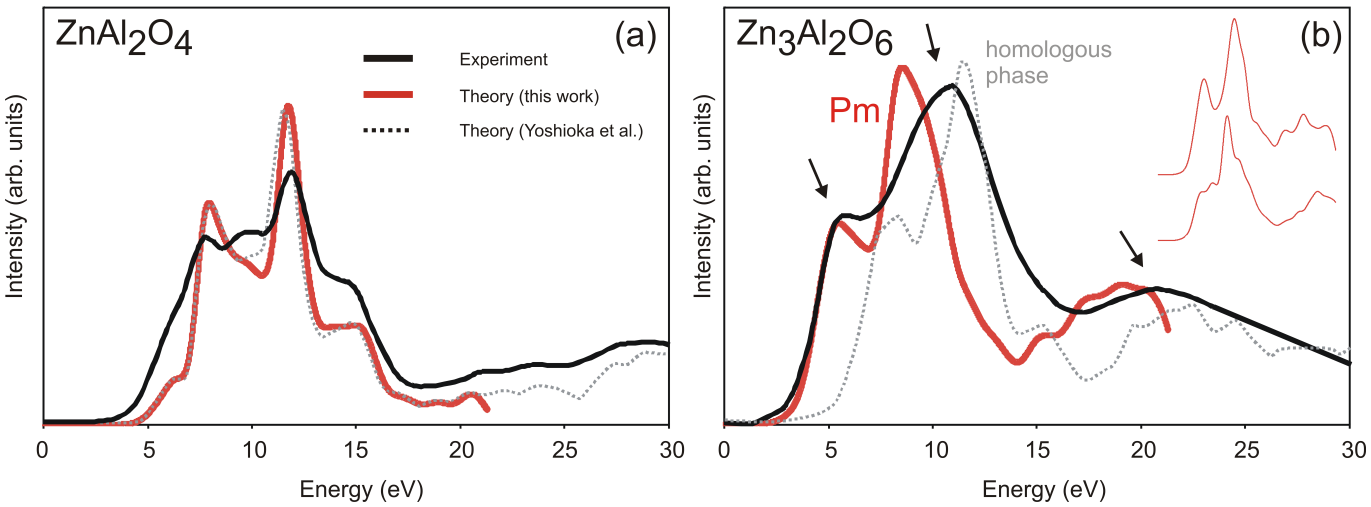

Fig. 3 Left: The theoretical Al K-edge XANES spectrum for $ZnAl_2O_4$ as calculated in this work (red) and by Ref.[23] (dotted grey), together with the experimental spectrum (black). Right: The experimental Al K-edge XANES spectrum for a concentrated Al-Zn-O solid solution with 19 at.% Al as produced by pulsed laser deposition (spectrum reproduced from Ref.[23]) (black, arrows indicate the three major features), compared with the theoretical XANES spectrum for the homologous phase (spectrum reproduced from Ref.[23]) (dotted grey) and with the theoretical XANES spectrum for the $Zn_3Al_2O_6$-crystal obtained from an evolutionary search (Tab. 1) (red). The latter is a sum of the two spectra that are shown in the inset, one for each of the two Al-sites.

tra that are better than the ones by a previous Zn-vacancy model, Yoshioka *et al.* point to the type of Al-coordination. In the Zn-vacancy model, only 4-fold oxygen coordinated Al sites appear. The homologous phase structure has a more rich behaviour, with 4-, 5- and 6-fold oxygen coordinate Al sites. A similar observation can be made for the new $Zn_3Al_2O_6$-structure, where the oxygen coordination turns out to be intermediate between 4-fold and 5-fold: neighbours appear at distances of 1.82 Å (2×), 1.87 Å, 1.90 Å and 1.96 Å for the first Al, and at 1.78 Å 1.81 Å (2×), 1.87 Å and 2.25 Å for the second Al. This has to be compared with a Al-O distance of 1.81 Å for substitutional (4-fold coordinated) Al in ZnO.

6 Conclusion

We apply an *ab initio* evolutionary search algorithm to a crystal engineering problem, and suggest by this way a metastable phase for $Zn_3Al_2O_6$ that has a formation energy that is lower than the one of any previously suggested crystal structure. Its local and overall structural features are consistent with the available experimental evidence (lattice expansion and XANES). We suggest this phase to be the one that is formed upon supersaturating ZnO with Al, which is responsible for the observed conductivity drop. This study demonstrates the increased levels of confidence and relevance that are achievable by using unbiased structure prediction tools. Due to the latter qualities, we expect *ab initio* evolutionary search will become a routine method in the toolbox of crystal engineering.

7 Acknowledgements

The authors acknowledge helpful discussions with Diederik Depla (Ghent University). This work received financial support from the IWT-Vlaanderen through the ISIMADE project. Calculations were carried out using the Stevin Supercomputer Infrastructure at Ghent University, funded by Ghent University, the Flemish Supercomputer Center (VSC), the Hercules Foundation, and the Flemish Government (EWI Department). S.C. acknowledges financial support from OCAS NV by an OCAS-endowed chair at Ghent University.

References

1 H. Ohta, K. Nomura, H. Hiramatsu, K. Ueda, T. Kamiya, M. Hirano and H. Hosono, *Solid-State Electronics*, 2003, **47**, 2261.
2 B. Ingram, G. Gonzalez, D. Kammler, M. Bertoni and T. Mason, *Journal of Electroceramics*, 2004, **13**, 167.
3 H. Hosono, *Thin Solid Films*, 2007, **515**, 6000.
4 E. Fortunato, D. Ginley, H. Hosono and D. C. Paine, *MRS Bulletin*, 2007, **32**, 242.
5 A. Walsh, J. L. D. Silva and S.-H. Wei, *Journal of Physics: Condensed Matter*, 2011, **23**, 334210.
6 R. G. Gordon, *MRS Bulletin*, 2000, **August**, 52.
7 A. V. Gavrilenko, K. Dondapati, V. I. Gavrilenko, J. Kim, G. V. Naik and A. Boltasseva, Proc. SPIE 8455, Metamaterials: Fundamentals and Applications V, 2012, p. 84552B.

8 H. Agura, A. Suzuki, T. Matsushita, T. Aoki and M. Okuda, *Thin Solid Films*, 2003, **445**, 263 – 267.

9 G. Granqvist Claes, *Solar Energy Materials and Solar Cells*, 2007, **91**, 1529–1598.

10 J. Elam, D. Routkevitch and S. Georgea, *Journal of the Electrochemical Society*, 2003, **150**,.

11 P. Banerjee, W.-J. Lee, K.-R. Bae, S. B. Lee and G. W. Rubloff, *Journal of Applied Physics*, 2010, **108**, 043504.

12 M. Čeh, H.-C. Chen, M.-J. Chen, J.-R. Yang and M. Shiojiri, *Materials Transactions*, 2010, **51**, 219.

13 D.-J. Lee, J.-Y. Kwon, S.-H. Kim, H.-M. Kim and K.-B. Kim, *Journal of The Electrochemical Society*, 2011, **158**, D277.

14 Y.-C. Cheng, *Applied Surface Science*, 2011, **258**, 604.

15 M. Sakamaki, N. Kawai, T. Miki, T. Kaneko, T. Konishi, T. Fujikawa, K. Amemiya, Y. Kitajima, Y. Kato, T. Muro, H. Yamauchi and M. Sakai, *Physical Review B*, 2011, **83**, 155210.

16 A. A. Letailleur, S. YuGrachev, E. Barthel, E. Sondergard, K. Nomenyo, C. Couteau, S. M. Murtry, G. Lérondel, E. Charlet and E. Peter, *Journal of Luminescence*, 2011, **131**, 2646.

17 T. Tsubota, M. Ohtaki, K. Eguchi and H. Arai, *Journal of Materials Chemistry*, 1997, **7**, 85.

18 M. H. Yoon, S. H. Lee, H. L. Park, H. K. Kim and M. S. Jang, *Journal of Materials Science Letters*, 2002, **21**, 1703.

19 R. Hansson, P. C. Hayes and E. Jak, *Metallic Materials Transactions B*, 2004, **35**, 633.

20 K. Shirouzu, T. Ohkusa, M. Hotta, N. Enomoto and J. Hojo, *Journal of the Ceramic Society of Japan*, 2007, **115**, 254–258.

21 H. Serier, M. Gaudon and M. Ménétrier, *Solid State Sciences*, 2009, **11**, 1192–1197.

22 G. Lu J., Z. Ye Z., J. Zeng Y., P. Zhu L., L. Wang, J. Yuan, H. Zhao B. and L. Liang Q., *Journal of Applied Physics*, 2006, **100**, 3714.

23 S. Yoshioka, F. Oba, R. Huang, I. Tanaka, T. Mizoguchi and T. Yamamoto, *Journal of Applied Physics*, 2008, **103**, 014309.

24 S. Yoshioka, K. Toyoura, F. Oba, A. Kuwabara, K. Matsunaga and I. Tanaka, *Journal of Solid State Chemistry*, 2008, **181**, 137.

25 S. Cornelius, M. Vinnichenko, N. Shevchenko, A. Rogozin, A. Kolitsch and W. Möller, *Journal of Applied Physics*, 2009, **94**, 042103.

26 M. Jullien, D. Horwat, F. Manzeh, R. E. Galindo, P. Bauer, J. Pierson and J. Endrino, *Solar Energy Materials and Solar Cells*, 2011, **95**, 2341 – 2346.

27 D. Horwat, M. Jullien, F. Capon, J. Pierson, J. Andersson and J. Endrino, *Journal of Physics D: Applied Physics*, 2010, **43**, 132003.

28 M. Vinnichenko, R. Gago, S. Cornelius, N. Shevchenko, A. Rogozin, A. Kolitsch, F. Munnik and W. Möller, *Applied Physics Letters*, 2010, **96**, 141907.

29 A. R. Oganov and C. W. Glass, *J Chem Phys*, 2006, **124**, 244704.

30 N. L. Abraham and M. I. J. Probert, *Phys. Rev. B*, 2006, **73**, 224104.

31 A. N. Kolmogorov, S. Shah, E. R. Margine, A. F. Bialon, T. Hammerschmidt and R. Drautz, *Phys. Rev. Lett.*, 2010, **105**, 217003.

32 P. Hohenberg and W. Kohn, *Phys. Rev.*, 1964, **136**, B864–B871.

33 W. Kohn and L. J. Sham, *Phys. Rev.*, 1965, **140**, A1133–A1138.

34 S. Cottenier, *Density Functional Theory and the Family of (L)APW-methods: a step-by-stey introduction*, Instituut voor Kern- en Stralingsfysica, KU Leuven, Belgium, 2002.

35 J. P. Perdew, K. Burke and M. Ernzerhof, *Phys. Rev. Lett.*, 1996, **77**, 3865.

36 J. P. Perdew, K. Burke and M. Ernzerhof, *Phys. Rev. Lett.*, 1997, **78**, 1396.

37 P. E. Blöchl, *Phys. Rev. B*, 1994, **50**, 17953.

38 G. Kresse and D. Joubert, *Phys. Rev. B*, 1999, **59**, 1758.

39 G. Kresse and J. Furthmüller, *Phys. Rev. B*, 1996, **54**, 11169.

40 E. Sjöstedt, L. Nordström and D. Singh, *Solid State Communications*, 2000, **114**, 15.

41 G. K. H. Madsen, P. Blaha, K. Schwarz, E. Sjöstedt and L. Nordström, *Phys. Rev. B*, 2001, **64**, 195134.

42 P. Blaha, K. Shwarz, G. K. H. Madsen, D. Kvasnicka and J. Luitz, *WIEN2k, An Augmented Plane Wave + Local Orbitals program for Calculating Crystal Properties*, Karlheinz Schwarz, Techn. Universität Wien, Austria, 2001.

43 M. Valle and A. R. Oganov, *Acta Crystallogr. A*, 2010, **66**, 507–517.

44 R. Allmann and R. Hinek, *Acta Crystallographica Section A*, 2007, **63**, 412–417.

45 S. Grazulis, D. Chateigner, R. T. Downs, A. F. T. Yokochi, M. Quirós, L. Lutterotti, E. Manakova, J. Butkus, P. Moeck and A. L. Bail, *Journal for Applied Crystallography*, 2009, **42**, 726.

46 http://www.crystallography.net.